

1  
2  
3  
4  
5  
6  
7  
8  
9  
10  
11  
12  
13  
14  
15  
16  
17  
18  
19  
20  
21  
22  
23  
24  
25  
26  
27  
28  
29  
30  
31  
32  
33  
34  
35  
36  
37  
38  
39  
40  
41  
42  
43  
44  
45  
46  
47  
48  
49  
50  
51  
52  
53  
54  
55  
56  
57  
58  
59  
60

# On the successes and opportunities for discovery of metal oxide photoanodes for solar fuels generators

*Lan Zhou,<sup>a</sup> Aniketa Shinde,<sup>a</sup> Dan Guevarra,<sup>a</sup> Joel A. Haber,<sup>a</sup> Kristin A. Persson,<sup>b,c,d</sup> Jeffrey B. Neaton,<sup>b,e,f</sup> John M. Gregoire<sup>a,g,\*</sup>*

<sup>a</sup> Joint Center for Artificial Photosynthesis, California Institute of Technology; Pasadena, California 91125, United States; <sup>b</sup> Joint Center for Artificial Photosynthesis, Lawrence Berkeley National Laboratory, Berkeley, CA 94720, United States; <sup>c</sup> Department of Materials Science and Engineering, University of California, Berkeley, CA 94720, United States; <sup>d</sup> Environmental Energy Technologies Division, Lawrence Berkeley National Laboratory; <sup>e</sup> Department of Physics, University of California, Berkeley, Berkeley, CA 94720, United States; <sup>f</sup> Molecular Foundry, Lawrence Berkeley National Laboratory, Berkeley, CA 94720, United States; Kavli Energy NanoSciences Institute, University of California, Berkeley, Berkeley, CA 94720, United States. <sup>g</sup> Division of Engineering and Applied Science, California Institute of Technology, Pasadena, CA 91125, United States

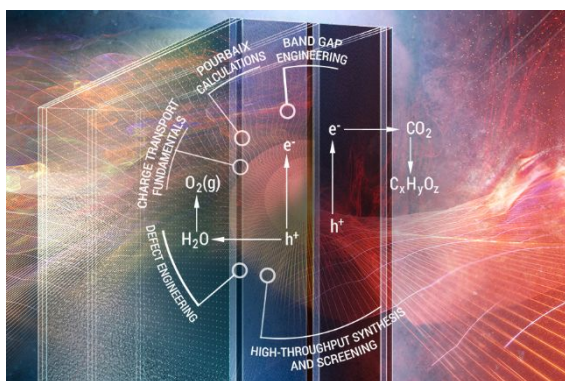
## Corresponding Author

\*gregoire@caltech.edu

ABSTRACT: The importance of metal oxide photoanodes in solar fuels technology has garnered concerted efforts in photoanode discovery in recent decades, which complement parallel efforts in

development of analytical techniques and optimization strategies using standard photoanodes such as  $\text{TiO}_2$ ,  $\text{Fe}_2\text{O}_3$  and  $\text{BiVO}_4$ . Theoretical guidance of high throughput experiments has been particularly effective in dramatically increasing the portfolio of metal oxide photoanodes, motivating a new era of photoanode development where the characterization and optimization techniques developed on traditional materials are applied to nascent photoanodes that exhibit visible light photoresponse. The compendium of metal oxide photoanodes presented in the present work can also serve as the basis for further technique development, with a primary goal to establish workflows for discovery of materials that perform better against the critical criteria of operational stability, visible light photoresponse, and photovoltage suitable for tandem absorber architectures.

## TOC GRAPHICS



The generation of chemicals and fuels from  $\text{CO}_2$ ,  $\text{N}_2$ , and  $\text{H}_2\text{O}$  in photoelectrochemical reactors would enable sustainable energy infrastructure with decreased reliance on photovoltaic and battery technologies that pose challenges for energy storage and transport.<sup>1</sup> The source chemical  $\text{CO}_2$  is used for generation of C-containing chemicals such as CO and formate as well as higher-order fuels such as liquid hydrocarbons and alcohols that could displace fossil-based liquid fuels while leveraging existing infrastructure.<sup>2</sup> The source chemical  $\text{N}_2$  is used for generation of  $\text{NH}_3$  and less

1  
2  
3 often  $\text{N}_2\text{H}_4$ , which may serve as fuels but can serve a more pressing need of sustainable fertilizer  
4 production.<sup>3</sup> These families of reactions involve electrochemical reduction of the source  
5 chemicals, generally referred to as  $\text{CO}_2$  reduction reactions ( $\text{CO}_2\text{RR}$ ) and  $\text{N}_2$  reduction reactions  
6 ( $\text{N}_2\text{RR}$ ), respectively. These reduction reactions require protons and electrons, and liberation of  
7 those reactants from  $\text{H}_2\text{O}$  via the  $\text{O}_2$  evolution reaction (OER) has been adopted as the primary  
8 strategy for establishing broadly-deployable solar fuels technologies. The  $\text{H}_2$  evolution reaction  
9 (HER) can also be coupled to the OER without  $\text{CO}_2$  or  $\text{N}_2$  reactants, making solar  
10 photoelectrocatalysis of the OER a cross-cutting technology for generation of  $\text{H}_2$ , C-containing,  
11 and N-containing fuels. Metal oxide photoanodes can also be used for anodic reactions other than  
12 the OER, resulting in synthesis of other chemicals,<sup>4</sup> although the present work considers solar fuels  
13 photoanodes to be photoelectrocatalysts for the OER in aqueous electrolyte.

14  
15 While photoelectrocatalysis of the HER and OER can occur with a single wide-gap  
16 semiconductor, as demonstrated in the seminal water splitting work utilizing  $\text{TiO}_2$ ,<sup>5</sup> the broad  
17 consensus, supported by multi-physics device modelling,<sup>6</sup> is that efficient utilization of the solar  
18 spectrum requires tandem light absorbers with band gap energies in the visible spectrum. While a  
19 number of device architectures utilizing a pair of visible-gap semiconductors have been proposed,  
20 a grand challenge of the solar fuels community has been the identification of a suitable solar fuels  
21 photoanode, i.e. a semiconductor that can utilize visible light to effect photoelectrocatalysis of the  
22 OER and circumvent a broad range of deactivation processes such as corrosion.

23  
24 Photovoltaic-grade semiconductors, most notably III-V semiconductors, have enabled a variety  
25 of high efficiency solar water splitting demonstrations.<sup>7</sup> While protective coating<sup>8</sup> of photovoltaic  
26 semiconductors has been effective in increasing operational stability from minutes to over 100  
27 hours,<sup>7</sup> semiconductors that don't self-passivate under operational conditions will always be

1  
2  
3 susceptible to device failure upon damage in the protective coating(s). This type of single point  
4 failure is difficult to circumvent in systems engineering and can render the technology untenable  
5 for deployment. Intrinsic stability of the semiconductors is the most reliable way to achieve a  
6 durable solar fuels generator, which has motivated the persistent and continuing effort to  
7 understand metal oxide semiconductors and identify those that can serve as solar fuels  
8 photoanodes. No fundamental limit on the efficiency of metal oxide photoanodes has been  
9 established beyond those dictated by the thermodynamics of solar energy conversion, and BiVO<sub>4</sub>-  
10 based devices with ca. 5% efficiency are approaching these limits given its 2.4 eV band gap.<sup>9</sup>  
11 Photoanode band gap energies no larger than 2 eV are required to realize the 15%-20% solar to  
12 fuel conversion efficiencies, the target range per technoeconomic and device models,<sup>6, 10</sup> requiring  
13 the community to pursue a combination of low band gap energy and high radiative efficiency that  
14 has yet to be approached by metal oxide photoanodes.  
15  
16  
17  
18  
19  
20  
21  
22  
23  
24  
25  
26  
27  
28  
29

30 To establish the outlook for this grand challenge, we first summarize the progress to date. Recent  
31 reviews have highlighted a broad portfolio of materials, techniques and devices. Abdi and  
32 Berglund<sup>11</sup> recently reviewed metal oxide photoanodes with focus on the optimization of BiVO<sub>4</sub>  
33 and its implementation into water splitting devices, along with summary of several other V, W and  
34 Fe-based oxide photoanodes, covering in total 9 metal oxide photoanode phases. Chu et al.<sup>12</sup>  
35 focused more on classes of materials and the integration of photoelectrodes into devices. He et  
36 al.<sup>13</sup> compiled a more detailed survey of metal oxide photoanodes with 33 phases discussed and  
37 critical analysis of several topics including the electronic character of the conduction and valence  
38 bands and other electronic structure considerations. Our literature survey, summarized in Fig. 1  
39 and detailed in the SI, identified 109 OER metal oxide photoanode phases, including recent  
40 discoveries from our labs. Of these, we find 70 visible light-active phases, corresponding to  
41  
42  
43  
44  
45  
46  
47  
48  
49  
50  
51  
52  
53  
54  
55  
56  
57  
58  
59  
60

1  
2  
3 photoanodes demonstrated to be photoactive with only sub-3 eV illumination.<sup>§</sup> The breadth of  
4  
5 elements utilized in photoanode studies is rapidly expanding, and the number of visible light-active  
6  
7 metal oxide photoanodes has increased 5-fold in the past 20 years, an acceleration in discovery  
8  
9 driven by the concerted efforts in the community, including our high throughput discovery  
10  
11 program in the Joint Center for Artificial Photosynthesis (JCAP). During these 20 years, there has  
12  
13 also been substantial effort to develop and deploy the present champion visible-gap metal oxide  
14  
15 photoanode, BiVO<sub>4</sub>.<sup>11, 14</sup> These parallel community efforts in discovery of new metal oxide  
16  
17 photoanodes and in optimization and understanding of BiVO<sub>4</sub>, both of which have been  
18  
19 remarkably successful, provide the framework for the future of the field.  
20  
21  
22  
23

24 BiVO<sub>4</sub> is an exemplar of a complex metal-oxide, visible-light photoanode whose study has  
25  
26 established the basis for accelerating development of metal oxide photoanodes.<sup>15</sup> In addition to  
27  
28 optimization schemes such as defect engineering for charge transport and selective carrier  
29  
30 extraction,<sup>16</sup> research on BiVO<sub>4</sub> has resulted in development of a broad range of materials and  
31  
32 device-level solar fuels characterization techniques.<sup>17</sup> A recent review of strategies for enhancing  
33  
34 the photocurrent, photovoltage, and stability of photoelectrodes highlights the breadth and  
35  
36 effectiveness of feedback between synthesis and characterization of device-relevant parameters to  
37  
38 optimize materials, as illustrated in Fig. 2.<sup>17</sup> The breadth of these materials development strategies  
39  
40 far exceeds the breadth of candidate photoanodes for which they have been deployed. The general  
41  
42 bias in scientific research towards continued investigation of well-researched materials is both  
43  
44 broadly known and recently evaluated as a limitation on creativity and discovery,<sup>18</sup> motivating our  
45  
46 effort in the present work to establish the set of known visible light-active photoanodes and discuss  
47  
48 opportunities for improving performance both within this set of materials and beyond, via new  
49  
50 materials discovery strategies.  
51  
52  
53  
54  
55  
56  
57  
58  
59  
60

1  
2  
3 Of the 70 visible light-active metal oxide photoanodes, historically  $\text{Fe}_2\text{O}_3$  and more recently  
4  $\text{BiVO}_4$  are arguably the only materials for which the community has deeply invested in detailed  
5 understanding and optimization, motivating further study on the other 68 phases, or some  
6 principled selection of a subset thereof. Some notable efforts in this area include detailed  
7 experimental investigation of  $\alpha\text{-SnWO}_4$ ,<sup>19</sup>  $\text{Fe}_2\text{WO}_6$ ,<sup>20</sup> copper vanadates such as  $\beta\text{-Cu}_2\text{V}_2\text{O}_7$  and  $\gamma\text{-}$   
8  $\text{Cu}_3\text{V}_2\text{O}_8$ ,<sup>21</sup> and computational investigation of  $\beta\text{-Cu}_2\text{V}_2\text{O}_7$ <sup>22</sup> to elucidate performance-limiting  
9 properties. Of these, only the copper vanadates exhibit a photon energy onset of photoactivity near  
10 2 eV, the desired upper-limit described above. Fig. 3 summarizes the photon energy onset for 49  
11 metal oxide photoanodes that exhibit external quantum efficiency (EQE) in excess of 0.01% in our  
12 experiments. Two notable phases with photoactivity at 2.1 eV (but insufficient to meet the EQE  
13 threshold) are  $\text{VCrO}_4\text{-orth}$ <sup>23</sup> and  $\text{V}_2\text{CoO}_6\text{-tri}$ .<sup>24</sup> The 4 phases that exceed the threshold at 2.1 eV  
14 are  $\text{FeBiO}_3$ , discovered by Chen et al.,<sup>25</sup> as well as  $\text{FeWO}_4$ ,<sup>26</sup>  $\gamma\text{-V}_2\text{Cu}_3\text{O}_8$ ,<sup>27</sup> and  $\text{Y}_3\text{Fe}_5\text{O}_{12}$ ,<sup>24</sup>  
15 highlighting the challenge of identifying metal oxide photoanodes with broad spectral response. A  
16 chopped illumination voltage sweep is shown for each of these 4 phases, demonstrating that the  
17 photocurrent decreases quickly with decreasing bias for most phases. Anecdotal examples  
18 demonstrating improvement in operational photovoltage, i.e. beyond that exhibited in this figure,  
19 include the observation of a turn on potential (lowest potential with observed photocurrent) near  
20 0.6 V vs RHE for  $\text{FeBiO}_3$ <sup>25</sup> and near 0.4 V vs RHE for Bi-alloyed  $\text{FeWO}_4$ .<sup>26</sup> More detailed  
21 understanding of the semiconductor-liquid junctions and band energy alignment are needed to  
22 elucidate the limiting photovoltage and associated efficiency of each photoanode, as discussed  
23 further below.

24  
25  
26  
27  
28  
29  
30  
31  
32  
33  
34  
35  
36  
37  
38  
39  
40  
41  
42  
43  
44  
45  
46  
47  
48  
49  
50  
51 With regards to the opportunity space for further discovery, it is interesting to consider the  
52 fraction of the metal oxide search space that has been explored. The 70 visible light photoanodes  
53  
54  
55  
56  
57  
58  
59  
60

1  
2  
3 utilize 25 cation elements from the periodic table. Considering only ternary metal oxides, which  
4  
5 account for all but 6 of these phases, only 34 of the 300 pairwise combinations of these cations  
6  
7 have been reported. While some may have been explored without discovery, most remain  
8  
9 uncharted territory. High Throughput (HiTp) experimental screening of OER photoanodes,  
10  
11 pioneered by Parkinson<sup>28</sup> and McFarland<sup>29</sup> and advanced by others,<sup>30</sup> accelerates exploration of  
12  
13 this broad class of photoanode candidates, although the search space remains too large to be  
14  
15 comprehensively searched with brute force screening. Our research has, thus, focused on guidance  
16  
17 of high throughput experiments via theory-based identification of promising materials systems for  
18  
19 photoanode discovery.  
20  
21  
22

23  
24 The photoanodes identified by our high throughput screening (see SI) include 4 copper vanadates  
25  
26 that were identified simultaneously by HiTp theory and experiment.<sup>23</sup> These initial discoveries  
27  
28 motivated theory screening of Materials Project entries<sup>31</sup> based on electronic structure and stability,  
29  
30 leading to experimental demonstration of photoanodic activity in 8 additional ternary metal  
31  
32 vanadates<sup>32</sup> and 5 ternary metal manganates.<sup>27</sup> Experimental screening in composition spaces  
33  
34 related to these theory predictions resulted in the identification of an additional 29 photoanode  
35  
36 phases.<sup>24, 33</sup> Perhaps the most important lesson from this work is that computational screening not  
37  
38 only identifies target phases but also promising composition regions that are sufficiently specific  
39  
40 to enable exploration by HiTp experiments, which are in turn sufficiently broad in scope to identify  
41  
42 materials beyond the computational search.  
43  
44  
45

46  
47 The fringe cases in these photoanode discovery campaigns offer insights for guiding future  
48  
49 discovery efforts.  $\text{FeWO}_4$  was identified through combinatorial investigation of non-equilibrium  
50  
51 synthesis conditions.<sup>26</sup> This  $\text{Fe}^{+2}$ -containing metal oxide is stabilized against oxidation by a self-  
52  
53 passivation surface layer that includes  $\text{Fe}^{+3}$ , highlighting the role of self-passivation in enabling  
54  
55  
56  
57  
58  
59  
60

1  
2  
3 stable operation of thermodynamically unstable photoanodes. Self-passivation was also observed  
4  
5 in copper vanadates, where the degradation in photocurrent was found to depend on the thickness  
6  
7 of the developed passivating film.<sup>34</sup> Passive surface films are of intense interest in the metals and  
8  
9 alloy industry and provide a fruitful research area in themselves as their formation and  
10  
11 functionality are still not entirely understood.<sup>35</sup> A range of phenomenological models have been  
12  
13 developed to explain the evolution of passivation layers, which display varying morphology, short-  
14  
15 range order and chemical constitution depending on the growth process and chemical  
16  
17 environment.<sup>36</sup> The stability of a passivating surface film, and hence that of the underlying bulk  
18  
19 material, is explicitly linked to ionic transport through the film which in turn depends critically on  
20  
21 the film morphology. Establishing thermodynamic and kinetic criteria for classifying a photoanode  
22  
23 as being operationally stable and supporting photoelectrocatalysis is a key area for designing the  
24  
25 next-generation of photoanode screening. In previous work,<sup>34, 37</sup> we have found that well-  
26  
27 benchmarked Pourbaix diagrams<sup>38</sup> can provide a qualitative guide as to the likely formation of, as  
28  
29 well as general chemical composition of, a passive surface film. Furthermore, first-principles  
30  
31 methods have been shown to provide quantitative estimates for the relative Gibbs free energy and  
32  
33 corresponding aqueous regimes where a candidate photoanode material may form inert passivating  
34  
35 films, or steadily corrode to aqueous species.<sup>37</sup> Detailed understanding of the growth process,  
36  
37 evolution, and structure of these complex, self-passivation films is presently lacking, motivating  
38  
39 development of new computational and experimental techniques that lead to a predictive model  
40  
41 for how the near-surface of a given material will evolve under operational conditions.  
42  
43  
44  
45  
46  
47  
48

49 The heterogeneous composition and structure of the photoanode as a function of depth from the  
50  
51 electrolyte surface complicates the already complex model of semiconductor-liquid junctions, as  
52  
53 the effect on these surface layers on band alignment and carrier transport have been insufficiently  
54  
55  
56  
57  
58  
59  
60



1  
2  
3 studied to date. The standard thermodynamic requirement of band alignment, i.e. the vacuum  
4 energy of the photoanode's valence band being sufficiently negative such that the photo-generated  
5 holes are sufficiently oxidizing to drive the OER, is complicated by electrolyte pH-dependent  
6 surface dipoles.<sup>39</sup> The polar surfaces of metal oxides introduce the additional complications of  
7 facet and termination-dependent dipoles that alter this band alignment, as exemplified by  
8  $\text{BiMn}_2\text{O}_5$ <sup>40</sup> where band level calculations for each of 6 low-energy surfaces indicate more than 1.4  
9 eV variation in work function, making the assessment of band alignment with respect to OER as  
10 much of a property of the surface as it is of the bulk electronic structure. Further study of facet-  
11 dependent and interfacial layer-dependent properties are likely to identify optimal photoanode  
12 surfaces and guide synthesis and device implementation by designating desirable and undesirable  
13 facets at the electrolyte interface. Initial demonstrations of this concept include facet-dependent  
14 charge separation in  $\text{BiVO}_4$ <sup>41</sup> and  $\text{SrTiO}_3$ .<sup>42</sup>

15  
16  
17  
18  
19  
20  
21  
22  
23  
24  
25  
26  
27  
28  
29  
30  
31 This aforementioned  $\text{BiMn}_2\text{O}_5$ ,<sup>40</sup> as well as  $\beta\text{-Mn}_2\text{V}_2\text{O}_7$ ,<sup>43</sup> provide additional opportunity to  
32 investigate performance-limiting attributes of metal oxide photoanodes. The 1.8 eV direct gap of  
33 each phase is ideal with respect to solar absorption, but they have yet to be demonstrated as OER  
34 photoanodes. While operational stability is a prime suspect for a lack of photoactivity, these are  
35 among the most electrochemically stable low-gap metal oxides, with Pourbaix-stable regions in  
36 the approximate ranges 0.3-0.7 and 0.3-1.2 V vs RHE, respectively. Despite these desirable  
37 attributes, these phases are not classified as photoanodes in the present work due to their  
38 photoactivity only in the presence of sacrificial hole acceptors. The modest photoactivity obtained  
39 with sacrificial hole acceptors also indicates that the photoanode performance limitations extend  
40 beyond poor OER catalysis. From an electronic structure point of view, these are exemplary  
41 photoanode candidates, motivating detailed inspection as to whether materials optimization can  
42  
43  
44  
45  
46  
47  
48  
49  
50  
51  
52  
53  
54  
55  
56  
57  
58  
59  
60

1  
2  
3 confer higher photoactivity, and/or identification of fundamental properties that limit photoactivity  
4  
5 with commensurate design of associated screening techniques.  
6

7  
8 Ternary manganate phases also illustrate the challenges of treating high-temperature or  
9  
10 disordered magnetic states in electronic structure calculations. For these ternary manganates, zero-  
11  
12 temperature calculations with judiciously-chosen magnetic configurations were required to gauge  
13  
14 the possible electronic structure of each phase's ambient temperature paramagnetic state;<sup>40, 43</sup>  
15  
16 paramagnetic states, in which the local magnetic moments on each open-shell cation are nonzero  
17  
18 but their configurational average is zero, are not trivially-compatible with periodic supercells.  
19  
20 Typically, high-throughput computational screening employs a computationally less expensive  
21  
22 model of the magnetic state, e.g. the ferromagnetic configuration, which can induce significant  
23  
24 changes to the electronic structure<sup>44</sup> of the material compared to the paramagnetic state. In our  
25  
26 experience, this approximation can lead to exclusion of promising low-gap metal oxides that  
27  
28 exhibit a metallic character in their ferromagnetic state. Antiferromagnetic (AF) ordering is  
29  
30 typically a better approximation of the paramagnetic state, and currently the Materials Project is  
31  
32 pursuing a large computational survey of the magnetic state of its materials including at least one  
33  
34 AF ordering for each transition metal oxide.<sup>44</sup> Other approaches for computational modelling of  
35  
36 paramagnetic materials have been introduced in the literature,<sup>45</sup> creating an opportunity to evaluate  
37  
38 the electronic structure of photoanode materials at relevant operating temperatures.  
39  
40  
41  
42  
43

44  
45 The compendium of photoanode phases described in the SI offers various opportunities for  
46  
47 identifying trends and descriptors for photoactivity. A seldom-discussed materials property that is  
48  
49 well characterized by our combinatorial experiments is cation off-stoichiometry of metal oxide  
50  
51 photoanodes. Fig. 4 shows the EQE under 3.2 eV illumination for 55  $A_{1-x}B_x$  oxide phases, where  
52  
53 B is taken to be the higher valent cation produced by the Materials Project oxidation state  
54  
55  
56  
57  
58  
59  
60

1  
2  
3 interpreter, and each phase is plotted by the difference in  $x$  between XRF measurements of thin  
4 film composition and that of the formula unit (FU). In addition to showing the considerable  
5 variation in EQE over the collection of metal oxide photoanodes, the observation of appreciable  
6 EQE at substantial composition deviations is quite striking. There are 5 phases with composition  
7 deviation more than 0.18 from the composition of the prototype structure. With this level of  
8 composition deviation, nanocrystalline secondary phases (not detected by XRD) may be present,  
9 although such composition differences often occur with a multi-valent cation such that the host  
10 structure can support substantial alloying. For example, the phases with an excess of the higher  
11 valent cation include formal valences  $A^{+2}$  ( $A = \text{Ca}$  or  $\text{Mg}$ ) and either  $\text{Mn}^{+3}$  or  $\text{Mn}^{+4}$ , where excess  
12 Mn appears to alloy as  $\text{Mn}^{+2}$  on the  $A^{+2}$  site. There are also cases where the structure of interest is  
13 only observed in off-stoichiometric conditions, such as  $\text{V}_2\text{Ag}_{0.33}\text{O}_5$  where an excess of Ag is  
14 needed to form the structure under our synthesis conditions, likely resulting in some metallic Ag  
15 in the thin film sample. This level of off-stoichiometry in solar energy conversion materials has  
16 been most extensively studied with Cu-based p-type semiconductors such as  $\text{Cu}(\text{In,Ga})\text{Se}_2$ ,<sup>46</sup>  
17  $\text{Cu}_2\text{SnZnS}_4$ ,<sup>47</sup> and  $\text{CuBi}_2\text{O}_4$ <sup>48</sup> where alloyed variants improve phase stability with respect to  
18 competing phases and/or alter the electronic structure. These phenomena underlie the composition  
19 variations of photoanodes in Fig. 4, where alloying can additionally optimize a catalytic activity  
20 and/or electrochemical passivation.  
21  
22  
23  
24  
25  
26  
27  
28  
29  
30  
31  
32  
33  
34  
35  
36  
37  
38  
39  
40  
41  
42  
43

44 The uncertainty in the XRF compositions is nominally 5 at.%, so phases appearing outside the  
45  $\pm 0.06$  window are confidently off-stoichiometric, bringing into question whether traditional  
46 methods would discover these photoanodes. Of the 23 such phases, 7 are also photoactive within  
47 the  $\pm 0.06$  window, so discovery may have been possible with synthesis at a composition matching  
48 the target FU. The remaining 16 phases required composition deviation to be discovered in our  
49  
50  
51  
52  
53  
54  
55  
56  
57  
58  
59  
60

1  
2  
3 experiments, highlighting the utility of composition libraries in photoanode discovery and  
4  
5 motivating further study of how substantial alloying optimizes photoanode performance.  
6

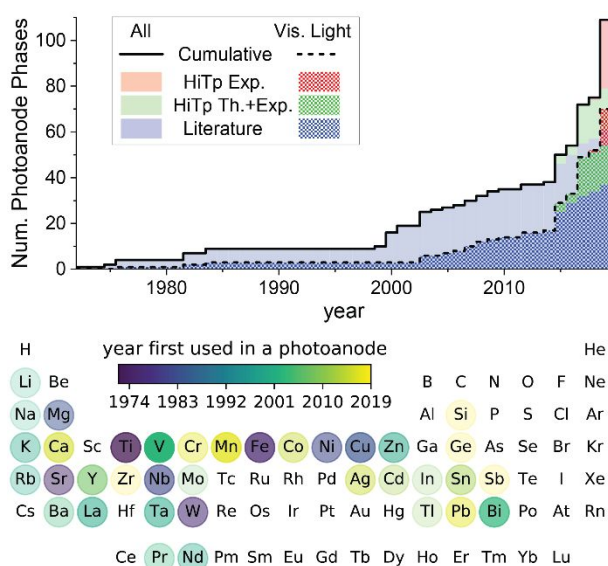
7  
8 Intertwined with the cation off-stoichiometry is the oxygen stoichiometry, or oxygen vacancy  
9  
10 concentration, which is not amenable to high throughput characterization, resulting in a lack of  
11  
12 observable trends over the set of known photoanodes. Recent work on  $\text{BiVO}_4$  has demonstrated  
13  
14 that over various time scales, the sub-band-gap states created by oxygen vacancies trap holes and  
15  
16 electrons, ultimately requiring thermal de-trapping to produce photoactivity.<sup>49</sup> These results  
17  
18 highlight the complexity of carrier transport in metal oxide photoanodes, which often involves  
19  
20 small polaron hopping<sup>50</sup> and may additionally involve more complex phenomena over a range of  
21  
22 time scales. An opportunity arising from these recent advances is determination of the extent to  
23  
24 which the observed conduction mechanisms of  $\text{BiVO}_4$  are universal to ternary vanadates and other  
25  
26 metal oxide photoanodes, and if the electronic structure contributions of oxygen vacancies, for  
27  
28 example, can be used as a functional descriptor of metal oxide photoanodes. Our HiTp screening  
29  
30 work includes a concerted exploration of ternary vanadates where we demonstrated tuning of band  
31  
32 gap energies across the visible range through band edge hybridization with various open-d-shell  
33  
34 cations.<sup>23</sup> These are specific examples of a general property of metal oxide photoanodes: nontrivial  
35  
36 orbital character (particularly d orbital character) at band edges creates opportunities for tuning the  
37  
38 band-edge electronic structure in new ways, potentially leading to electron and hole conductivities  
39  
40 that are not well described by semi-classical, Boltzmann-based band transport theory.  
41  
42  
43  
44  
45

46  
47 Traditional semiconductor characterization of conductivity or effective carrier mobility is  
48  
49 necessary but insufficient for specific identification of the transport-limiting phenomenon. Recent  
50  
51 developments in ultrafast spectroscopy have demonstrated direct observation of polaron  
52  
53 formation,<sup>51</sup> and application of such techniques to a broader class of photoanodes will help  
54  
55  
56  
57  
58  
59  
60

1  
2  
3 establish trends in the roles of defects, excited states, etc. in metal oxide semiconductor transport.  
4  
5 Disentangling the transport mechanisms can also be facilitated by theory, although the highly-  
6  
7 localized and strongly correlated electronic states (e.g. states with d orbital character) typically  
8  
9 require rigorous treatment beyond that of standard theories and computational methods. Metal  
10  
11 oxides often exhibit such electronic states, and as noted above, photoanodes of interest often  
12  
13 encompass additional structural and chemical complexity that may alter transport properties and  
14  
15 may require treatment of many-atom systems, creating substantial computational expense.  
16  
17 Although DFT calculations are often used to compute band structures in practice, rigorous  
18  
19 calculations of spectroscopic properties of metal oxide photoanode candidates require formalisms  
20  
21 beyond the ground-state, time-independent DFT. In materials physics, the formalism of choice for  
22  
23 quantitative prediction of the band structure and optical properties is *ab initio* many-body  
24  
25 perturbation theory (MBPT).<sup>52</sup> MBPT has been historically computationally prohibitive for  
26  
27 complex materials, but it is beginning to be applied to complex systems, such as the metal oxide  
28  
29 photoanodes BiVO<sub>4</sub> and  $\beta$ -Cu<sub>2</sub>V<sub>2</sub>O<sub>7</sub>,<sup>22, 53</sup> and interfaces involving photoanode materials and  
30  
31 water.<sup>54</sup> Additionally, detailed *ab initio* calculations of photoexcited carrier dynamics, limited by  
32  
33 phonon scattering, are now possible for simple semiconductors,<sup>55</sup> and have more recently been  
34  
35 extended to oxides.<sup>56</sup> A growing number of recent methodologies are being proposed for more  
36  
37 rigorous calculations of polaron formation energies.<sup>57</sup> Collectively, advances in these methods  
38  
39 promise a significantly deeper and richer understanding and assessment of photogenerated carrier  
40  
41 phenomena in existing candidate photoanodes, which will also lead to new descriptors for  
42  
43 discovery of photoelectrode materials.  
44  
45  
46  
47  
48  
49

50  
51 Solar fuels photoanodes pose substantial challenges for materials discovery due to the combined  
52  
53 needs of solar absorption, charge carrier separation and transport, chemical and electrochemical  
54  
55  
56  
57  
58  
59  
60

1  
2  
3 stability under operating conditions, as well as catalytic activity for the OER. The recent increase  
4  
5 in chemical diversity of metal oxide photoanodes presents both challenges, for example  
6  
7 determining which phases are amenable to optimization and integration into solar fuels generators,  
8  
9 and opportunities, for example developing new theory and experiment campaigns to better  
10  
11 understand fundamental properties that give rise to photoanodic activity. Despite the prolific  
12  
13 photoanode discovery efforts of the last 20 years, solar fuels photoanodes are still rare compared  
14  
15 to other types of functional materials, motivating continued identification of such materials to  
16  
17 formulate models that relate fundamental materials properties to photoanode performance,  
18  
19 enhancing scientific understanding as well as development of deployable solar fuels materials. The  
20  
21 photoactivity of off-stoichiometric variants of phases is notable, motivating application of defect  
22  
23 and transport characterization techniques, which have been recently developed via study of  $\text{Fe}_2\text{O}_3$   
24  
25 and  $\text{BiVO}_4$ , to a broader set of metal oxide phases. Combining the recent proliferation of both  
26  
27 photoanode discoveries and advanced characterization techniques will advance fundamental  
28  
29 understanding of metal oxide photoelectrocatalysts and the design of next-generation photoanodes.  
30  
31  
32  
33  
34



35  
36  
37  
38  
39  
40  
41  
42  
43  
44  
45  
46  
47  
48  
49  
50  
51  
52  
53 Figure 1: (top) Summary of OER photoanodes from literature (blue), as well as our previous  
54  
55 reports integrating HiTp theory and experiment (green) and additional HiTp experiment  
56  
57  
58  
59  
60

discoveries (red). (bottom) Using all photoanodes, the year in which each element was first used in a photoanode is shown on the periodic table, with the saturation of each circle corresponding to the number of times the element appears in the list of 109 photoanodes.

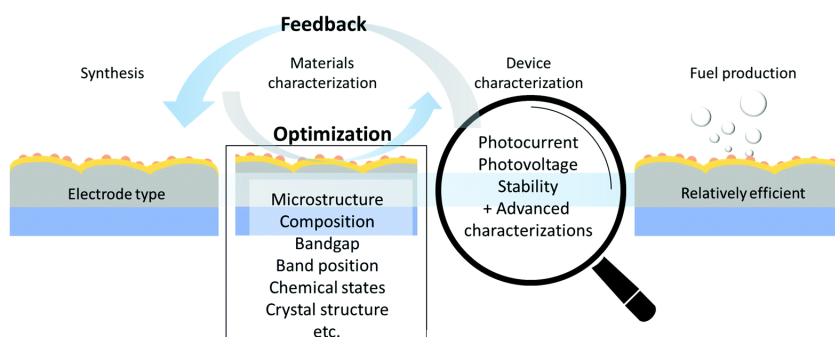


Figure 2: Illustration of synthesis and processing-based optimization of a library of materials properties, with feedback provided by an ever-expanding suite of materials and device-level characterizations. Adapted from Ref. <sup>17</sup> with permission.

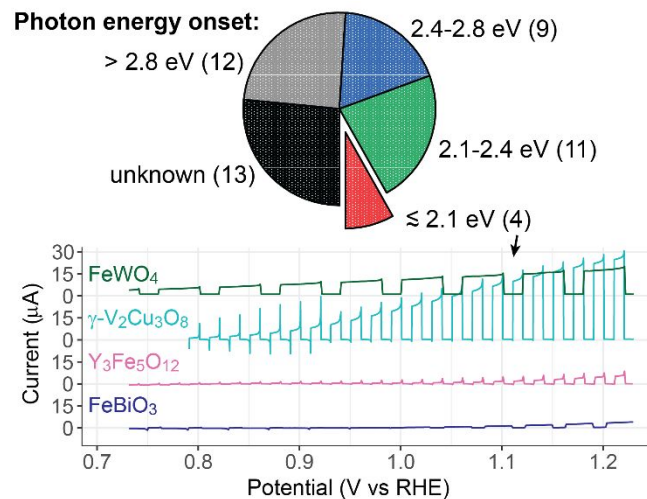


Figure 3: The pie chart shows the distribution of photon energy onset for photoactivity, for 49 metal oxide photoanode phases from combinatorial libraries with EQE in excess of 0.01% (see SI). The photon energy onset is determined via photoelectrochemistry at 1.23 V vs RHE with a

series of light emitting diodes, and due to their spectral breadth the boundaries between the 4 ranges have ca.  $\pm 0.1$  eV uncertainty. For the 4 photoanodes with photoactivity at 2.1 eV, the cathodic sweep from a cyclic voltammogram is shown with toggled 3.2 eV illumination (variable illumination intensity, see SI). These data were acquired in pH 13 (0.1 M NaOH) for  $\gamma$ - $V_2Cu_3O_8$  and  $Y_3Fe_5O_{12}$  and borate-buffered pH 9.3 electrolyte for  $FeWO_4$  and  $FeBiO_3$ , as reported previously.<sup>24, 26-27</sup>

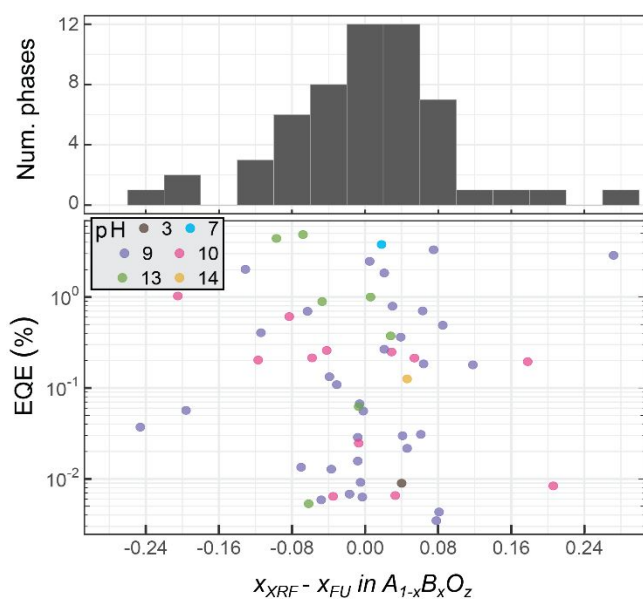


Figure 4: Summary of 55 photoanode phases from combinatorial libraries with available XRF measurement of composition. For each identified ternary oxide, the cation stoichiometry  $x$  is taken as  $A_{1-x}B_xO_z$  where B is generally the higher valent cation. The quantity  $x_{XRF} - x_{FU}$  is the difference in  $x$  between the composition of the most photoactive sample and that of the formula unit. The EQE at 3.2 eV is shown as the metric for photoactivity as this is the only illumination source used for all photoanode samples.

ASSOCIATED CONTENT



1  
2  
3 **Supporting Information.** Table of 109 metal oxide photoanodes from the literature survey  
4 summarized in Fig. 1. Table of HiTp composition and photoelectrochemical data for 58 phases  
5  
6 measured in our labs.  
7  
8  
9

10  
11 **AUTHOR INFORMATION**  
12

13  
14 \*gregoire@caltech.edu  
15  
16

17 **Notes**  
18

19  
20 The authors declare no competing financial interest.  
21  
22

23 § In the literature survey, photoactivity under white light illumination combined with optical  
24 identification of a sub-2.8 eV band gap was considered to be sufficient evidence for a visible  
25 light photoanode.  
26  
27  
28  
29

30  
31 **AUTHOR BIOGRAPHIES**  
32

33 Lan Zhou earned her Ph.D in Materials Science from University of Vermont in 2010, and is  
34 currently working as a Staff Scientist in the High Throughput Experimentation group at Caltech.  
35 Her research focuses on developing processes for combinatorial materials synthesis of metals,  
36 metal oxides, and mixed anion materials used in solar-fuels applications.  
37  
38  
39  
40  
41  
42

43 Aniketa Shinde specializes in instrumentation, materials science, and electrochemistry for energy  
44 research. Her focus is high-throughput scanning drop sensor measurements for  
45 photoelectrochemical and electrochemical characterization of thin films. She received her Master's  
46 and PhD degrees in Physics from the University of California, Irvine.  
47  
48  
49  
50  
51  
52

53 Dan Guevarra has been a member of the High Throughput Experimentation group and the Joint  
54 Center for Artificial Photosynthesis at Caltech since 2013. He received a Master of Information  
55  
56  
57  
58  
59  
60

1  
2  
3 and Data Science from the University of California, Berkeley and presently works on data analysis,  
4  
5 visualization, machine learning, and instrument automation.  
6  
7

8  
9 Joel A. Haber is a Staff Scientist at the California Institute of Technology in the Joint Center for  
10  
11 Artificial Photosynthesis. His research focuses on inorganic materials chemistry and high-  
12  
13 throughput materials science, as applied to materials and devices for solar-energy conversion.  
14  
15

16  
17 Kristin A. Persson is an Associate Professor in Materials Science and Engineering at UC Berkeley  
18  
19 with a joint appointment as Senior Faculty Scientist at the Lawrence Berkeley National  
20  
21 Laboratory. She is also the Director of the Materials Project ([www.materialsproject.org](http://www.materialsproject.org)) and  
22  
23 specializes in materials informatics and data-driven design of novel materials.  
24  
25

26  
27 Jeffrey B. Neaton is a Professor of Physics at UC Berkeley, and Senior Faculty Scientist and  
28  
29 Associate Laboratory Director for Energy Sciences at Lawrence Berkeley National Laboratory.  
30  
31 He is also a member of the Kavli Energy Nanosciences Institute at Berkeley. His research focuses  
32  
33 on the development and application of electronic structure theory for predictive calculations of  
34  
35 properties of inorganic and organic energy and quantum materials.  
36  
37

38  
39 John Gregoire is the Thrust Coordinator for Photoelectrocatalysis in the Joint Center for Artificial  
40  
41 Photosynthesis, a U.S. DOE Energy Innovation Hub. He leads the High Throughput  
42  
43 Experimentation group at Caltech, which accelerates scientific discovery by automating critical  
44  
45 components of materials research workflows, from synthesis to data interpretation.  
46  
47  
48  
49  
50

51  
52 **ACKNOWLEDGMENT**  
53  
54  
55  
56  
57  
58  
59  
60

1  
2  
3 This material is based upon work performed by the Joint Center for Artificial Photosynthesis, a  
4  
5 DOE Energy Innovation Hub, supported through the Office of Science of the U.S. Department of  
6  
7 Energy under Award Number DE-SC0004993.  
8  
9

## 10 QUOTES TO HIGHLIGHT

11  
12  
13 Theoretical guidance of high throughput experiments has been particularly effective in  
14 dramatically increasing the portfolio of metal oxide photoanodes, motivating a new era of  
15 photoanode development where the characterization and optimization techniques developed on  
16 traditional materials are applied to nascent photoanodes that exhibit visible light photoresponse.  
17  
18

19 Computational screening not only identifies target phases but also promising composition  
20 regions that are sufficiently specific to enable exploration by high throughput experiments,  
21 which are in turn sufficiently broad in scope to identify materials beyond the computational  
22 search.  
23

24 The photoactivity of off-stoichiometric variants of phases is notable, motivating application of  
25 defect and transport characterization techniques, which have been recently developed via study  
26 of Fe<sub>2</sub>O<sub>3</sub> and BiVO<sub>4</sub>, to a broader set of metal oxide phases.  
27  
28

29 Combining the recent proliferation of both photoanode discoveries and advanced  
30 characterization techniques will advance fundamental understanding of metal oxide  
31 photoelectrocatalysts and the design of next-generation photoanodes.  
32  
33

## 34 REFERENCES

- 35  
36  
37 1. Kraan, O.; Kramer, G. J.; Haigh, M.; Laurens, C., An Energy Transition That Relies Only  
38 on Technology Leads to a Bet on Solar Fuels. *Joule* **2019**, *3* (10), 2286-2290.  
39  
40 2. Raciti, D.; Wang, C., Recent Advances in CO<sub>2</sub> Reduction Electrocatalysis on Copper.  
41 *ACS Energy Letters* **2018**, *3* (7), 1545-1556.  
42  
43 3. Chen, X.; Li, N.; Kong, Z.; Ong, W.-J.; Zhao, X., Photocatalytic fixation of nitrogen to  
44 ammonia: state-of-the-art advancements and future prospects. *Materials Horizons* **2018**, *5* (1), 9-  
45 27.  
46  
47 4. Sayama, K., Production of High-Value-Added Chemicals on Oxide Semiconductor  
48 Photoanodes under Visible Light for Solar Chemical-Conversion Processes. *ACS Energy Letters*  
49 **2018**, *3* (5), 1093-1101.  
50  
51 5. Mavroides, J. G.; Tchernev, D. I.; Kafalas, J. A.; Kolesar, D. F., Photoelectrolysis of  
52 water in cells with TiO<sub>2</sub> anodes. *Materials Research Bulletin* **1975**, *10* (10), 1023-1030.  
53  
54 6. Fountaine, K. T.; Lewerenz, H. J.; Atwater, H. A., Efficiency Limits for  
55 Photoelectrochemical Water-Splitting. *Nat. Commun.* **2016**, *7*, 13706.  
56  
57 7. Tournet, J.; Lee, Y.; Karuturi, S. K.; Tan, H. H.; Jagadish, C., III–V Semiconductor  
58 Materials for Solar Hydrogen Production: Status and Prospects. *ACS Energy Letters* **2020**, 611-  
59 622.  
60

8. Bae, D.; Seger, B.; Vesborg, P. C. K.; Hansen, O.; Chorkendorff, I., Strategies for stable water splitting via protected photoelectrodes. *Chem Soc Rev* **2017**, *46* (7), 1933-1954.
9. Kim, J. H.; Han, S.; Jo, Y. H.; Bak, Y.; Lee, J. S., A precious metal-free solar water splitting cell with a bifunctional cobalt phosphide electrocatalyst and doubly promoted bismuth vanadate photoanode. *Journal of Materials Chemistry A* **2018**, *6* (3), 1266-1274.
10. Sathre, R.; Greenblatt, J. B.; Walczak, K.; Sharp, I. D.; Stevens, J. C.; Ager, J. W.; Houle, F. A., Opportunities to improve the net energy performance of photoelectrochemical water-splitting technology. *Energ Environ Sci* **2016**, *9* (3), 803-819.
11. Abdi, F. F.; Berglund, S. P., Recent developments in complex metal oxide photoelectrodes. *Journal of Physics D: Applied Physics* **2017**, *50* (19), 193002.
12. Chu, S.; Li, W.; Yan, Y.; Hamann, T.; Shih, I.; Wang, D.; Mi, Z., Roadmap on solar water splitting: current status and future prospects. *Nano Futures* **2017**, *1* (2), 022001.
13. He, H.; Liao, A.; Guo, W.; Luo, W.; Zhou, Y.; Zou, Z., State-of-the-art progress in the use of ternary metal oxides as photoelectrode materials for water splitting and organic synthesis. *Nano Today* **2019**, 100763.
14. (a) Sayama, K.; Nomura, A.; Zou, Z. G.; Abe, R.; Abe, Y.; Arakawa, H., Photoelectrochemical Decomposition of Water on Nanocrystalline BiVO<sub>4</sub> Film Electrodes Under Visible Light. *Chem. Commun.* **2003**, (23), 2908-2909; (b) Lamm, B.; Trześniewski, B. J.; Döscher, H.; Smith, W. A.; Stefik, M., Emerging Postsynthetic Improvements of BiVO<sub>4</sub> Photoanodes for Solar Water Splitting. *ACS Energy Letters* **2018**, *3* (1), 112-124; (c) Kim, J. H.; Lee, J. S., Elaborately Modified BiVO<sub>4</sub> Photoanodes for Solar Water Splitting. *Advanced Materials* **2019**, *31* (20), 1806938.
15. Sharp, I. D.; Cooper, J. K.; Toma, F. M.; Buonsanti, R., Bismuth Vanadate as a Platform for Accelerating Discovery and Development of Complex Transition-Metal Oxide Photoanodes. *ACS Energy Letters* **2017**, *2* (1), 139-150.
16. Zhang, W.; Liu, M., Modulating Carrier Transport via Defect Engineering in Solar Water Splitting Devices. *ACS Energy Letters* **2019**, *4* (4), 834-843.
17. Yang, W.; Prabhakar, R. R.; Tan, J.; Tilley, S. D.; Moon, J., Strategies for enhancing the photocurrent, photovoltage, and stability of photoelectrodes for photoelectrochemical water splitting. *Chem Soc Rev* **2019**, *48* (19), 4979-5015.
18. Jia, X.; Lynch, A.; Huang, Y.; Danielson, M.; Lang'at, I.; Milder, A.; Ruby, A. E.; Wang, H.; Friedler, S. A.; Norquist, A. J.; Schrier, J., Anthropogenic biases in chemical reaction data hinder exploratory inorganic synthesis. *Nature* **2019**, *573* (7773), 251-255.
19. Kölbach, M.; Pereira, I. J.; Harbauer, K.; Plate, P.; Höflich, K.; Berglund, S. P.; Friedrich, D.; van de Krol, R.; Abdi, F. F., Revealing the Performance-Limiting Factors in  $\alpha$ -SnWO<sub>4</sub> Photoanodes for Solar Water Splitting. *Chem Mater* **2018**, *30* (22), 8322-8331.
20. Abdi, F. F.; Chemseddine, A.; Berglund, S. P.; van de Krol, R., Assessing the Suitability of Iron Tungstate (Fe<sub>2</sub>WO<sub>6</sub>) as a Photoelectrode Material for Water Oxidation. *The Journal of Physical Chemistry C* **2017**, *121* (1), 153-160.
21. Jiang, C.-M.; Segev, G.; Hess, L. H.; Liu, G.; Zaborski, G.; Toma, F. M.; Cooper, J. K.; Sharp, I. D., Composition-Dependent Functionality of Copper Vanadate Photoanodes. *ACS Applied Materials & Interfaces* **2018**, *10* (13), 10627-10633.
22. Wiktor, J.; Reshetnyak, I.; Strach, M.; Scarongella, M.; Buonsanti, R.; Pasquarello, A., Sizable Excitonic Effects Undermining the Photocatalytic Efficiency of  $\beta$ -Cu<sub>2</sub>V<sub>2</sub>O<sub>7</sub>. *The Journal of Physical Chemistry Letters* **2018**, *9* (19), 5698-5703.

23. Yan, Q.; Yu, J.; Suram, S. K.; Zhou, L.; Shinde, A.; Newhouse, P. F.; Chen, W.; Li, G.; Persson, K. A.; Gregoire, J. M.; Neaton, J. B., Solar fuels photoanode materials discovery by integrating high-throughput theory and experiment. *Proceedings of the National Academy of Sciences of the United States of America* **2017**, *114* (12), 3040-3043.
24. Zhou, L.; Shinde, A.; Guevarra, D.; Richter, M. H.; Stein, H. S.; Wang, Y.; Newhouse, P.; Persson, K.; Gregoire, J., Combinatorial screening yields discovery of 29 metal oxide photoanodes for solar fuel generation. *Journal of Materials Chemistry A* **2020**, 10.1039/C9TA13829C.
25. Chen, X. Y.; Yu, T.; Gao, F.; Zhang, H. T.; Liu, L. F.; Wang, Y. M.; Li, Z. S.; Zou, Z. G.; Liu, J. M., Application of weak ferromagnetic BiFeO<sub>3</sub> films as the photoelectrode material under visible-light irradiation. *Appl. Phys. Lett.* **2007**, *91* (2).
26. Zhou, L.; Shinde, A.; Suram, S. K.; Stein, H. S.; Bauers, S. R.; Zakutayev, A.; DuChene, J. S.; Liu, G.; Peterson, E. A.; Neaton, J. B.; Gregoire, J. M., Bi-Containing n-FeWO<sub>4</sub> Thin Films Provide the Largest Photovoltage and Highest Stability for a Sub-2 eV Band Gap Photoanode. *ACS Energy Letters* **2018**, *3* (11), 2769-2774.
27. Zhou, L.; Yan, Q.; Shinde, A.; Guevarra, D.; Newhouse, P. F.; Becerra-Stasiewicz, N.; Chatman, S. M.; Haber, J. A.; Neaton, J. B.; Gregoire, J. M., High Throughput Discovery of Solar Fuels Photoanodes in the CuO–V<sub>2</sub>O<sub>5</sub> System. *Adv. Energy Mater.* **2015**, *5*, 1500968.
28. (a) Woodhouse, M.; Herman, G. S.; Parkinson, B. A., Combinatorial Approach to Identification of Catalysts for the Photoelectrolysis of Water. *Chem. Mater.* **2005**, *17* (17), 4318-4324; (b) Rowley, J. G.; Do, T. D.; Cleary, D. A.; Parkinson, B. A., Combinatorial Discovery Through a Distributed Outreach Program: Investigation of the Photoelectrolysis Activity of p-Type Fe, Cr, Al Oxides. *ACS Applied Materials & Interfaces* **2014**, *6* (12), 9046-9052.
29. Jaramillo, T. F.; Baeck, S. H.; Kleiman-Shwarsstein, A.; Choi, K. S.; Stucky, G. D.; McFarland, E. W., Automated electrochemical synthesis and photoelectrochemical characterization of Zn<sub>1-x</sub>Co<sub>x</sub>O thin films for solar hydrogen production. *J. Comb. Chem.* **2005**, *7* (2), 264-271.
30. (a) Gutkowski, R.; Khare, C.; Conzuelo, F.; Kayran, Y. U.; Ludwig, A.; Schuhmann, W., Unraveling compositional effects on the light-induced oxygen evolution in Bi(V-Mo-X)O<sub>4</sub> material libraries. *Energ Environ Sci* **2017**, *10* (5), 1213-1221; (b) Meyer, R.; Sliozberg, K.; Khare, C.; Schuhmann, W.; Ludwig, A., High-Throughput Screening of Thin-Film Semiconductor Material Libraries II: Characterization of Fe-W-O Libraries. *ChemSusChem* **2015**, *8* (7), 1279-1285; (c) Lee, J. W.; Ye, H. C.; Pan, S. L.; Bard, A. J., Screening of photocatalysts by scanning electrochemical microscopy. *Anal. Chem.* **2008**, *80* (19), 7445-7450.
31. Jain, A.; Ong, S. P.; Hautier, G.; Chen, W.; Richards, W. D.; Dacek, S.; Cholia, S.; Gunter, D.; Skinner, D.; Ceder, G.; Persson, K. A., The Materials Project: A materials genome approach to accelerating materials innovation. *APL Materials* **2013**, *1* (1), 011002.
32. Shinde, A.; Suram, S. K.; Yan, Q.; Zhou, L.; Singh, A. K.; Yu, J.; Persson, K. A.; Neaton, J. B.; Gregoire, J. M., Discovery of Manganese-Based Solar Fuel Photoanodes via Integration of Electronic Structure Calculations, Pourbaix Stability Modeling, and High-Throughput Experiments. *ACS Energy Letters* **2017**, 2307-2312.
33. Noh, J.; Kim, S.; Gu, G. h.; Shinde, A.; Zhou, L.; Gregoire, J. M.; Jung, Y., Unveiling new stable manganese based photoanode materials via theoretical high-throughput screening and experiments. *Chemical Communications* **2019**, *55*, 13418-13421.
34. Zhou, L.; Yan, Q.; Yu, J.; Jones, R. J. R.; Becerra-Stasiewicz, N.; Suram, S. K.; Shinde, A.; Guevarra, D.; Neaton, J. B.; Persson, K. A.; Gregoire, J. M., Stability and Self-passivation of

- Copper Vanadate Photoanodes under Chemical, Electrochemical, and Photoelectrochemical Operation. *Phys. Chem. Chem. Phys.* **2016**, *18*, 9349-9352.
35. (a) Macdonald, D. D., On the Existence of Our Metals-Based Civilization: I. Phase-Space Analysis. *Journal of The Electrochemical Society* **2006**, *153* (7), B213-B224; (b) Macdonald, D. D., Passivity—the key to our metals-based civilization. *Pure and Applied Chemistry* **1999**, *71* (6), 951-978.
36. (a) Macdonald, D. D.; Urquidi-Macdonald, M., Theory of Steady-State Passive Films. *Journal of The Electrochemical Society* **1990**, *137* (8), 2395-2402; (b) Schultze, J. W.; Lohrengel, M. M., Stability, reactivity and breakdown of passive films. Problems of recent and future research. *Electrochim Acta* **2000**, *45* (15), 2499-2513.
37. Singh, A. K.; Zhou, L.; Shinde, A.; Suram, S. K.; Montoya, J. H.; Winston, D.; Gregoire, J. M.; Persson, K. A., Electrochemical Stability of Metastable Materials. *Chem Mater* **2017**, *29* (23), 10159-10167.
38. Persson, K. A.; Waldwick, B.; Lazic, P.; Ceder, G., Prediction of solid-aqueous equilibria: Scheme to combine first-principles calculations of solids with experimental aqueous states. *Phys. Rev. B* **2012**, *85* (23), 235438.
39. Stevanovic, V.; Lany, S.; Ginley, D. S.; Tumas, W.; Zunger, A., Assessing capability of semiconductors to split water using ionization potentials and electron affinities only. *Phys Chem Chem Phys* **2014**, *16* (8), 3706-3714.
40. Newhouse, P. F.; Reyes-Lillo, S. E.; Li, G.; Zhou, L.; Shinde, A.; Guevarra, D.; Suram, S. K.; Soedarmadji, E.; Richter, M. H.; Qu, X.; Persson, K.; Neaton, J. B.; Gregoire, J. M., Discovery and Characterization of a Pourbaix-Stable, 1.8 eV Direct Gap Bismuth Manganate Photoanode. *Chem Mater* **2017**, *29* (23), 10027-10036.
41. Li, R.; Han, H.; Zhang, F.; Wang, D.; Li, C., Highly efficient photocatalysts constructed by rational assembly of dual-cocatalysts separately on different facets of BiVO<sub>4</sub>. *Energ Environ Sci* **2014**, *7* (4), 1369-1376.
42. Mu, L.; Zhao, Y.; Li, A.; Wang, S.; Wang, Z.; Yang, J.; Wang, Y.; Liu, T.; Chen, R.; Zhu, J.; Fan, F.; Li, R.; Li, C., Enhancing charge separation on high symmetry SrTiO<sub>3</sub> exposed with anisotropic facets for photocatalytic water splitting. *Energ Environ Sci* **2016**, *9* (7), 2463-2469.
43. Yan, Q.; Li, G.; Newhouse, P. F.; Yu, J.; Persson, K. A.; Gregoire, J. M.; Neaton, J. B., Mn<sub>2</sub>V<sub>2</sub>O<sub>7</sub>: An Earth Abundant Light Absorber for Solar Water Splitting. *Advanced Energy Materials* **2015**, *5* (8), 1401840.
44. Horton, M. K.; Montoya, J. H.; Liu, M.; Persson, K. A., High-throughput prediction of the ground-state collinear magnetic order of inorganic materials using Density Functional Theory. *npj Computational Materials* **2019**, *5* (1), 64.
45. (a) Mozafari, E.; Alling, B.; Steneteg, P.; Abrikosov, I. A., Role of N defects in paramagnetic CrN at finite temperatures from first principles. *Physical Review B* **2015**, *91* (9), 094101; (b) Abrikosov, I. A.; Ponomareva, A. V.; Steneteg, P.; Barannikova, S. A.; Alling, B., Recent progress in simulations of the paramagnetic state of magnetic materials. *Current Opinion in Solid State and Materials Science* **2016**, *20* (2), 85-106; (c) Trimarchi, G.; Wang, Z.; Zunger, A., Polymorphous band structure model of gapping in the antiferromagnetic and paramagnetic phases of the Mott insulators MnO, FeO, CoO, and NiO. *Physical Review B* **2018**, *97* (3), 035107.
46. Ramanujam, J.; Singh, U. P., Copper indium gallium selenide based solar cells – a review. *Energy & Environmental Science* **2017**, *10* (6), 1306-1319.

- 1  
2  
3 47. Dhawale, D. S.; Ali, A.; Lokhande, A. C., Impact of various dopant elements on the  
4 properties of kesterite compounds for solar cell applications: a status review. *Sustainable Energy*  
5 *& Fuels* **2019**, *3* (6), 1365-1383.
- 6 48. Sharma, G.; Zhao, Z.; Sarker, P.; Nail, B. A.; Wang, J.; Huda, M. N.; Osterloh, F. E.,  
7 Electronic structure, photovoltage, and photocatalytic hydrogen evolution with p-CuBi<sub>2</sub>O<sub>4</sub>  
8 nanocrystals. *Journal of Materials Chemistry A* **2016**, *4* (8), 2936-2942.
- 9 49. Selim, S.; Pastor, E.; García-Tecedor, M.; Morris, M. R.; Francàs, L.; Sachs, M.; Moss,  
10 B.; Corby, S.; Mesa, C. A.; Gimenez, S.; Kafizas, A.; Bakulin, A. A.; Durrant, J. R., Impact of  
11 Oxygen Vacancy Occupancy on Charge Carrier Dynamics in BiVO<sub>4</sub> Photoanodes. *Journal of*  
12 *the American Chemical Society* **2019**, *141* (47), 18791-18798.
- 13 50. Rettie, A. J. E.; Chemelewski, W. D.; Emin, D.; Mullins, C. B., Unravelling Small-  
14 Polaron Transport in Metal Oxide Photoelectrodes. *The Journal of Physical Chemistry Letters*  
15 **2016**, *7* (3), 471-479.
- 16 51. Carneiro, L. M.; Cushing, S. K.; Liu, C.; Su, Y.; Yang, P.; Alivisatos, A. P.; Leone, S. R.,  
17 Excitation-wavelength-dependent small polaron trapping of photoexcited carriers in  $\alpha$ -Fe<sub>2</sub>O<sub>3</sub>.  
18 *Nature Materials* **2017**, *16* (8), 819-825.
- 19 52. (a) Strinati, G., Application of the Green's functions method to the study of the optical  
20 properties of semiconductors. *La Rivista del Nuovo Cimento (1978-1999)* **1988**, *11* (12), 1-86;  
21 (b) Onida, G.; Reining, L.; Rubio, A., Electronic excitations: density-functional versus many-  
22 body Green's-function approaches. *Reviews of Modern Physics* **2002**, *74* (2), 601-659; (c) Golze,  
23 D.; Dvorak, M.; Rinke, P., The GW Compendium: A Practical Guide to Theoretical  
24 Photoemission Spectroscopy. *Frontiers in Chemistry* **2019**, *7*, 377.
- 25 53. Wiktor, J.; Reshetnyak, I.; Ambrosio, F.; Pasquarello, A., Comprehensive modeling of  
26 the band gap and absorption spectrum of BiVO<sub>4</sub>. *Physical Review Materials* **2017**, *1* (2),  
27 022401.
- 28 54. (a) Ambrosio, F.; Wiktor, J.; Pasquarello, A., pH-Dependent Catalytic Reaction Pathway  
29 for Water Splitting at the BiVO<sub>4</sub>-Water Interface from the Band Alignment. *ACS Energy Letters*  
30 **2018**, *3* (4), 829-834; (b) Gerosa, M.; Gygi, F.; Govoni, M.; Galli, G., The role of defects and  
31 excess surface charges at finite temperature for optimizing oxide photoabsorbers. *Nature*  
32 *Materials* **2018**, *17* (12), 1122-1127.
- 33 55. (a) Bernardi, M.; Vigil-Fowler, D.; Lischner, J.; Neaton, J. B.; Louie, S. G., Ab Initio  
34 Study of Hot Carriers in the First Picosecond after Sunlight Absorption in Silicon. *Physical*  
35 *Review Letters* **2014**, *112* (25), 257402; (b) Bernardi, M.; Vigil-Fowler, D.; Ong, C. S.; Neaton,  
36 J. B.; Louie, S. G., Ab initio study of hot electrons in GaAs. *Proceedings of the National*  
37 *Academy of Sciences* **2015**, *112* (17), 5291-5296.
- 38 56. (a) Zhou, J.-J.; Hellman, O.; Bernardi, M., Electron-Phonon Scattering in the Presence of  
39 Soft Modes and Electron Mobility in SrTiO<sub>3</sub> Perovskite from First Principles. *Physical Review*  
40 *Letters* **2018**, *121* (22), 226603; (b) Zhou, J.-J.; Bernardi, M., Predicting charge transport in the  
41 presence of polarons: The beyond-quasiparticle regime in SrTiO<sub>3</sub>. *Physical Review Research*  
42 **2019**, *1* (3), 033138.
- 43 57. Sio, W. H.; Verdi, C.; Poncé, S.; Giustino, F., Polarons from First Principles, without  
44 Supercells. *Physical Review Letters* **2019**, *122* (24), 246403.
- 45  
46  
47  
48  
49  
50  
51  
52  
53  
54  
55  
56  
57  
58  
59  
60